J|A|C|S
ARTICLES
Published on Web 11/21/2003

$^{13}C-^{13}C$ Rotational Resonance Width Distance Measurements in Uniformly ^{13}C-Labeled Peptides

Ramesh Ramachandran, Vladimir Ladizhansky, Vikram S. Bajaj, and Robert G. Griffin*

Contribution from the Francis Bitter Magnet Laboratory and Department of Chemistry, Massachusetts Institute of Technology, Cambridge, Massachusetts 02139-4307

Received August 5, 2003; E-mail: rgg@mit.edu

Abstract: The rotational resonance width (R^2W) experiment is a constant-time version of the rotational resonance (R^2) experiment, in which the magnetization exchange is measured as a function of sample spinning frequency rather than the mixing time. The significant advantage of this experiment over conventional R^2 is that both the dipolar coupling and the relaxation parameters can be independently and unambiguously extracted from the magnetization exchange profile. In this paper, we combine R^2W with two-dimensional $^{13}C-^{13}C$ chemical shift correlation spectroscopy and demonstrate the utility of this technique for the site-specific measurement of multiple $^{13}C-^{13}C$ distances in uniformly labeled solids. The dipolar truncation effects, usually associated with distance measurements in uniformly labeled solids, are considerably attenuated in R^2W experiments. Thus, R^2W experiments are applicable to uniformly labeled biological systems. To validate this statement, multiple $^{13}C-^{13}C$ distances (in the range of 3−6 Å) were determined in *N*-acetyl-[U-^{13}C,^{15}N]L-Val-L-Leu with an average precision of ±0.5 Å. Furthermore, the distance constraints extracted using a two-spin model agree well with the X-ray crystallographic data.

Introduction

Recent innovations and technological advances in the field of solid-state NMR (SSNMR) spectroscopy have brought it to the point where it shows considerable promise as a technique for studying problems of biological relevance that are not accessible via solution NMR or diffraction techniques.[1−10] In particular, the combination of magic angle spinning (MAS),[11−13] cross-polarization (CP),[14,15] and heteronuclear decoupling techniques[16−18] yielded increased spectral resolution and sensitivity in studies of such systems. At the same time, MAS attenuates the dipolar interactions among the nuclear spins. Since these are the primary parameters of interest in structure determinations, it is necessary to reintroduce the dipolar interactions in order to retrieve the desired structural information. This fact has provided the impetus for the development of a suite of recoupling techniques that result in the reintroduction of the dipolar couplings during MAS in a controlled manner.[19−24] In such recoupling schemes (the rotational resonance technique considered here being an exception), the spin component of the dipolar interaction is modulated with radio frequency pulses to constructively interfere with the MAS modulated spatial component, thereby resulting in the reintroduction of the dipolar interaction. Using such approaches, distance constraints have been obtained in a number of selectively labeled systems.[20] These distance measurements are essential in determining the molecular structure of biological samples such as membrane proteins[2−5,25,26] and insoluble peptide aggregates,[9,10,27,28] whose

(1) McDermott, A.; Creuzet, F.; Griffin, R. G.; Zawadzke, L. E.; Ye, Q. Z.; Walsh, C. T. *Biochemistry* **1990**, *29*, 5567−5574.
(2) Creuzet, F.; McDermott, A.; Gebhard, R.; van der Hoef, K.; Spijker-Assink, M. B.; Herzfeld, J.; Lugtenburg, J.; Levitt, M. H.; Griffin, R. G. *Science* **1991**, *251*, 783−786.
(3) McDermott, A.; Creuzet, F.; Gebhard, R.; van der Hoef, K.; Levitt, M. H.; Herzfeld, J.; Lugtenburg, J.; Griffin, R. G. *Biochemistry* **1994**, *33*, 6129−6136.
(4) McDowell, L. M.; Klug, C. A.; Beusen, D. D.; Schaefer, J. *Biochemistry* **1996**, *35*, 5395−5403.
(5) McDowell, L. M.; Lee, M.; McKay, A.; Anderson, K. S.; Schaefer, J. *Biochemistry* **1996**, *35*, 3328−3334.
(6) Marassi, F. M.; Opella, S. J. *Curr. Opin. Struct. Biol.* **1998**, *8*, 640−648.
(7) Griffin, R. G. *Nature Struct. Biol.* **1998**, *5*, 508−512.
(8) Watts, A. *Curr. Opin. Biotech.* **1999**, *10*, 48−53.
(9) Tycko, R. *Curr. Opin. Chem. Biol.* **2000**, *4*, 500.
(10) Petkova, A. T.; Ishii, Y.; Balbach, J. J.; Antzutkin, O. N.; Leapman, R. D.; Delaglio, F.; Tycko, R. *Proc. Natl. Acad. Sci. U.S.A.* **2002**, *99*, 16742−16747.
(11) Andrew, E. R.; Bradbury, A.; Eades, R. G. *Nature* **1958**, *182*, 1659.
(12) Lowe, I. J. *Phys. Rev. Lett.* **1959**, *2*, 285.
(13) Long, J. R.; Sun, B. Q.; Bowen, A.; Griffin, R. G. *J. Am. Chem. Soc.* **1994**, *116*, 11950−11956.
(14) Pines, A.; Gibby, M. G.; Waugh, J. S. *J. Chem. Phys.* **1973**, *59*, 569−590.
(15) Schaefer, J. S.; Stejskal, E. O. *J. Am. Chem. Soc.* **1976**, *98*, 1030.
(16) Mehring, M.; Pines, A.; Rhim, W.-K.; Waugh, J. S. *J. Chem. Phys.* **1971**, *54*, 3239.
(17) Mehring, M.; Sinning, G. *Phys. Rev.* **1977**, *B15*, 2519−2532.
(18) Bennett, A. E.; Rienstra, C. M.; Auger, M.; Lakshmi, K. V.; Griffin, R. G. *J. Chem. Phys.* **1995**, *103*, 6951−6957.
(19) Bennett, A. E.; Griffin, R. G.; Vega, S. In *Solid State NMR IV: Methods and Applications of Solid-State NMR*; Blumich, B., Ed.; Springer-Verlag: Berlin, 1994; Vol.33, pp 1−77.
(20) Dusold, S.; Sebald, A. *Annu. Rep. Nucl. Magn. Reson. Spectrosc.* **2000**, *41*, 185−264.
(21) Hohwy, M.; Rienstra, C. M.; Jaroniec, C. P.; Griffin, R. G. *J. Chem. Phys.* **1999**, *110*, 7983−7992.
(22) Edén, M.; Levitt, M. H. *J. Chem. Phys.* **1999**, *111*, 1511−1519.
(23) Carravetta, M.; Edén, M.; Zhao, Z.; Brinkmann, A.; Levitt, M. H. *Chem. Phys. Lett.* **2000**, *321*, 205−215.
(24) Brinkmann, A.; Edén, M.; Levitt, M. H. *J. Chem. Phys.* **2001**, *115*, 357−384.
(25) Weliky, D. P.; Bennett, A. E.; Zvi, A.; Anglister, J.; Steinbach, P. J.; Tycko, R. *Nat. Struct. Biol.* **1999**, *6*, 141−145.
(26) (a) Jaroniec, C. P.; MacPhee, C. E.; Astrof, N. S.; Dobson, C. M.; Griffin, R. G. *Proc. Nat. Acad. Sci. USA* **2002**, *99*, 16748−16753. (b) Thompson, L. K.; McDermott, A. E.; Raap, J.; van der Wielen, C. M.; Lugtenburg, J.; Herzfeld, J.; Griffin, R. G. *Biochemistry* **1992**, *31*, 7931−7938.

structures are not easily accessible with conventional structural techniques such as solution-state NMR spectroscopy and X-ray crystallography.

Dipolar recoupling techniques can be conveniently classified as either broad-banded or selective. To date, broad-banded recoupling techniques are used extensively for spectral assignments, but the deleterious effects of dipolar truncation[29] and other multispin interactions on the spin dynamics limit their utility in distance measurements in uniformly ^{13}C labeled solids. In particular, the strong couplings among directly bonded spins attenuate polarization transfer to weakly coupled neighbors, and it is precisely these distances that are essential in structure determination. Quantifying multispin effects in uniformly labeled systems is difficult and usually results in inaccurate distance measurements. Moreover, such techniques are sensitive to pulse imperfections and require intense radio frequency modulations on the low-γ nuclei, which interfere with the proton decoupling, leading to a loss of signal intensity during the recoupling period.[30] In contrast, with selective recoupling techniques such as rotational resonance (R^2)[31−39] and its related variants,[40−43] such problems are circumvented because the applied rf fields are either weak or nonexistent.

In the case of R^2 experiments, the dipolar interaction between the members of a pair of spins is reintroduced selectively by matching the isotropic chemical shift difference, δ (in hertz), to an integer multiple of the sample spinning frequency (υ_r)—i.e., $\delta = n\upsilon_r$ (where n is a small integer representing the order of resonance)—and monitoring the exchange dynamics as a function of the mixing time. This leads to a coherent interaction between the nuclear spins and the macroscopic sample rotation, leading to magnetization exchange between the spins of interest. Since the recoupling during R^2 is rotor-driven, it is, in contrast to radio frequency driven recoupling techniques, less sensitive to interference from ^1H decoupling. Moreover, the spectral selectivity of the R^2 phenomenon is often advantageous in quantitative studies, as multiple and relayed polarization transfers are minimized. Most importantly, as a direct consequence of the selectivity, the dipolar truncation effects are significantly attenuated in R^2 experiments.

In addition to the dependence on the internuclear distance, the magnetization exchange dynamics at R^2 are sensitive to the homogeneous and inhomogeneous contributions to the zero quantum line-width parameters.[42−46] The homogeneous contribution is described by a phenomenological relaxation parameter T_2^{ZQ}, which characterizes the decay of the ZQ coherences created during the magnetization exchange. In addition, the chemical shift distribution (CSD)[47] represents an inhomogeneous contribution that arises mainly from variations in intermolecular packing and results in a distribution of chemical shifts at each of the recoupled spin sites. Quantifying these two zero-quantum contributions is an important and nontrivial task, since they must be separated from the dipolar couplings if structural parameters are to be measured accurately. Only recently have experiments been devised to measure the homogeneous and inhomogeneous contributions to such effects.[42,43,45,46,48−50]

In the usual R^2 magnetization exchange experiments, the dipolar couplings are extracted by fitting the experimental exchange curves with different sets of dipolar (and in some cases the magnitude and orientation of CSA tensors) and relaxation parameters. However, the accuracy of such distance measurements is limited by the accuracy with which the zero quantum line-width parameters (especially T_2^{ZQ}) are estimated and accounted for in the numerical simulations. The value of T_2^{ZQ} has a significant influence on the exchange dynamics and depending on its relative magnitude (with respect to the effective dipolar interaction), the form of the magnetization exchange trajectories vary from damped oscillations in the "underdamped" regime ($\omega_{eff} \gg 1/T_2^{ZQ}$) to monotonic decays in the opposite overdamped case ($\omega_{eff} \ll 1/T_2^{ZQ}$).[38] Short distances often fall in the underdamped category and can be measured accurately,[39] even without an accurate estimate of the zero quantum relaxation parameters. However, in the context of measurements intended to constrain the structure of biomolecules, the most interesting constraints arise from long-range dipolar contacts between residues that are also distant in the primary structure. These distances tend to correspond to the overdamped case. Consequently, the accuracy of such long-range distance measurements using the the R^2 magnetization exchange method can be significantly compromised by the uncertainties associated with the estimation of the ZQ relaxation parameters. This necessitates the need for developing experiments with a reduced dependence on the relaxation parameters.

With this goal in mind, Costa et al. proposed an experiment based on the rotational resonance technique where the magnetization exchange was monitored under a constant mixing time as a function of spinning frequency (rotational resonance width, R^2W),[43] which shows a reduced dependence on relaxation parameters. In a similar vein, Goobes et al.[45,46] proposed observation of the magnetization exchange as a function of spinning frequency in a constant time, narrow-band radio frequency driven recoupling (nb-RFDR) experiment. Both

(27) Gregory, D. M.; Benzinger, T. L. S.; Burkoth, T. S.; Miller-Auer, H.; Lynn, D. G.; Meredith, S. C.; Botto, R. E. *Solid State Nucl. Magn. Reson.* **1998**, *13*, 149−166.
(28) Tycko, R. *Annu. Rev. Phys. Chem.* **2001**, *52*, 575−606.
(29) Baldus, M.; Meier, B. H. *J. Magn. Reson.* **1997**, *128*, 172.
(30) Ishii, Y.; Ashida, J.; Terao, T. *Chem. Phys. Lett.* **1995**, *246*, 439−445.
(31) Andrew, E. R.; Clough, S.; Farnell, L. F.; Gledhill, T. A.; Roberts, I. *Phys. Lett.* **1966**, *21*, 505−506.
(32) Andrew, E. R.; Bradbury, A.; Eades, R. G.; Wynn. V. T *Phys. Lett.* **1963**, *4*, 99.
(33) Raleigh, D. P.; Harbison, S. G.; Neiss, J. E.; Roberts, J. E.; Griffin, R. G. *Chem. Phys. Lett.* **1987**, *138*, 285.
(34) Meier, B. H.; Earl, W. L. *J. Am. Chem. Soc.* **1987**, *109*, 7937.
(35) Raleigh, D. P.; Levitt, M. H.; Griffin, R. G. *Chem. Phys. Lett.* **1988**, *146*, 71−76.
(36) Colombo, M. G.; Meier, B. H.; Ernst, R. R. *Chem. Phys. Lett.* **1988**, *146*, 189.
(37) Raleigh, D. P.; Creuzet, F.; Das Gupta, S. K.; Levitt, M. H.; Griffin, R. G. *J. Am. Chem. Soc.* **1989**, *111*, 4502.
(38) Levitt, M. H.; Raleigh, D. P.; Creuzet, F.; Griffin, R. G. *J. Chem. Phys.* **1990**, *92*, 6347−6364.
(39) Williamson, P. T. F.; Verhoeven, A.; Ernst, M.; Meier, B. H. *J. Am. Chem. Soc.* **2003**, *125*, 2718−2722.
(40) Takegoshi, K.; Nomura, K.; Terao, T. *Chem. Phys. Lett.* **1995**, *232*, 424−428.
(41) Takegoshi, K.; Nomura, K.; Terao, T. *J. Magn. Reson.* **1997**, *127*, 206−216.
(42) Costa, P. R.; Sun, B.; Griffin, R. G. *J. Am. Chem. Soc.* **1997**, *119*, 10 821−10 836.
(43) Costa, P. R.; Sun, B.; Griffin, R. G. *J. Magn. Reson.* **2003**, *164*, 92−103.
(44) Kubo, A.; McDowell., C. A *J. Chem. Soc., Faraday Trans. 1* **1988**, *84*, 3713.
(45) Goobes, G.; Boender, G. J.; Vega, S. *J. Magn. Reson.* **2000**, *146*, 204−219.
(46) Goobes, G.; Vega, S. *J. Magn. Reson.* **2002**, *146*, 236−251.
(47) Vander Hart, D. L.; Earl, W. L.; Garroway, A. N. *J. Magn. Reson.* **1981**, *44*, 361.
(48) Karlsson, T.; Levitt, M. H. *J. Chem. Phys.* **1998**, *109*, 5493−5507.
(49) Karlsson, T.; Brinkmann, A.; Verdegem, P. J. E.; Lugtenburg, J.; Levitt, M. H. *Solid State Nucl. Magn. Reson.* **1999**, *14*, 43−58.
(50) Helmle, M.; Lee, Y. K.; Verdegem, P. J. E.; Feng, X.; Karlsson, T.; Lugtenburg, J.; de Groot, H. J. M.; Levitt, M. H. *J. Magn. Reson.* **1999**, *140*, 379−403.

approaches involve the observation of the ZQ resonance transition, with its intensity and width dependent on the dipolar coupling and relaxation parameters. The simultaneous analysis of both (or alternatively the resonance shape) allows independent extraction of distance and relaxation parameters without ambiguity when compared to the conventional R^2 experiments. Using this technique, internuclear distances in selectively labeled samples have been determined with a reduced dependence on zero-quantum line-width parameters and with much improved accuracy and precision.

The primary aim of the experiments reported here is to extend the applicability of the R^2W technique to uniformly ^{13}C-labeled systems and to investigate the dependence of the accuracy of R^2W measurements in the presence of multiple spin couplings. To address these issues, we have measured multiple distance constraints (in the range of 3−6 Å) in the dipeptide *N*-acetyl-[U-^{13}C,^{15}N]L-Val-L-Leu using 3D dipolar-chemical shift correlation spectroscopy. Using an approximate model of the spin dynamics that considers only two coupled spins, a total of 9 distances were extracted in good agreement with the diffraction distances. The excellent agreement of all the measured distances with X-ray data justifies the use of this simplified model. The ability of the R^2W approach to separate the effects of relaxation and dipolar couplings, and simultaneously attenuate dipolar truncation, makes it an invaluable tool in structural studies of uniformly labeled biological systems.

Experimental Section

The experiments were performed on a sample *N*-acetyl-[U-^{13}C,^{15}N]-L-valine-L-leucine (the *N*-acetyl group was not labeled). For measuring intramolecular distances, the above uniformly labeled compound was diluted to 9% in natural abundance to attenuate intermolecular dipolar couplings. The NMR spectra were recorded at 8.4 T (360.336 MHz for ^1H, 90.607 MHz for ^{13}C) using a Cambridge Instruments spectrometer (courtesy of Dr. D. J. Ruben) with a commercial Chemagnetics triple resonance MAS probe. The probe was equipped with a 4.0 mm Chemagnetics spinning module. Spinning frequencies in the range 5.8−7.5 kHz were used in the experiments and were regulated to ±2 Hz with a Bruker spinning frequency controller. The standard approach for site-specific measurement of multiple $^{13}C-^{13}C$ distances is illustrated in Figure 1a. Ramped cross-polarization[51] from ^1H creates the initial ^{13}C magnetization. The magnetization is then encoded by the t_1 evolution, followed by a preparatory $\pi/2$ pulse, which creates the initial longitudinal polarization (along the *z*-axis) for dipolar mixing. The second $\pi/2$ pulse creates transverse polarization for detection. The period between the two $\pi/2$ pulses constitutes the dipolar mixing time and is maintained constant in the experiment. In our implementation of the R^2W experiment, a series of two-dimensional experiments are performed using different sample spinning frequencies. Due to the larger ^{13}C spectral width, the t_1 increments in such 2D experiments are generally short in order to avoid spectral folding. Since the total number of scans is limited by the number of t_1 points (which in turn is needed to establish high resolution in the indirect dimension) as well as by phase cycling, such experiments are often time consuming, unnecessarily in small peptides where high signal-to-noise can be expected. This problem, however, can be circumvented by employing the pulse sequence illustrated in Figure 1b and has been implemented in our experiments. Here, following $^1H-^{13}C$ CP, the carbonyl region of the ^{13}C spectrum is selected by a 90° Gaussian pulse, which restores the $^{13}C{=}O$ magnetization to the *z*-axis of the rotating frame. This is followed by application of a *z*-filter, during which all unwanted coherences are dephased via transverse relaxation processes and removed through phase

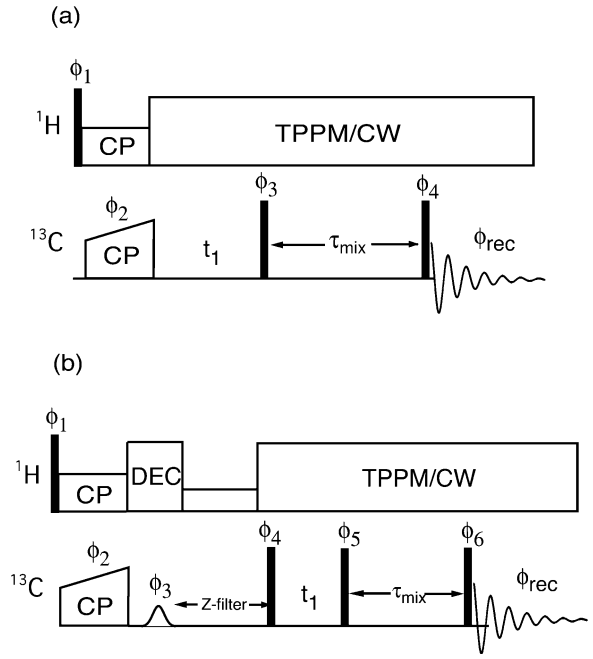

Figure 1. Pulse sequences for 3D-R^2W experiment. Solid rectangles represent $\pi/2$ pulses. (a) Represents a general $^{13}C-^{13}C$ correlation experiment performed as a function of spinning frequency with the following phase cycling scheme: $\varphi_1 = 1$, $\varphi_2 = 1313$, $\varphi_3 = 2$, $\varphi_4 = 1122, 3344$, $\varphi_{rec} = 1324, 3142, 3142, 1324$. (b) In this scheme a selective Gaussian flip-up pulse is employed to select the carbonyl region of the spectrum. The following phase cycles were employed: $\varphi_1 = 8 \times 1, 8 \times 3$; $\varphi_2 = 1$; $\varphi_3 = 8 \times 2, 8 \times 4$; $\varphi_4 = 1$; $\varphi_5 = 4 \times 3, 4 \times 1$; $\varphi_6 = 1234$; $\varphi_{rec} = 1234, 3412, 3412, 1234, 3412, 1234, 1234\ 3412$. The labels 1, 2, 3, 4 correspond to the phases $x, y, -x, -y$, respectively. In all the above experiments the phase of the ^1H-CP pulse was fixed along the *y*-axis and the dipolar mixing time (τ_{mix}) was 30 ms.

cycling. After the dephasing period, the carbonyl magnetization is restored to the transverse plane by a $\pi/2$ pulse. Since the spectral width of the residual ^{13}C (only carbonyl region) spectrum is reduced, larger t_1 increments are possible during the evolution period, thereby minimizing the total acquisition time. The chemical shifts of the carbonyl resonances are then encoded during t_1 evolution, which is then followed by a preparatory $\pi/2$ pulse for the magnetization exchange. The influence of the heteronuclear $^{13}C-^1H$ dipolar interaction during the t_1 evolution, $^{13}C-^{13}C$ recoupling period and acquisition is minimized by employing the two-pulse phase modulation (TPPM) decoupling scheme[18] (∼83 kHz, $\phi = 12°$, $\tau = 6\ \mu s$), while CW proton decoupling of ∼ 100 kHz was employed during the $\pi/2$ pulses. The length of ^{13}C $\pi/2$ pulses was 5 μs, and Gaussian pulse of 300 μs and recycle delays of 3 s were employed in all our experiments.

Numerical Simulations. The spin dynamics under rotational resonance conditions have been well described by several authors[34,36,38,40−43,48,50] and will not be considered in detail in this article. We therefore only present modifications of the theory relevant to our experimental scheme. In the high-field approximation, the spin Hamiltonian for an isolated spin pair during MAS is given by

$$H = \omega_1(t)I_{1z} + \omega_2(t)I_{2z} + \omega_d(t)[2I_{1z}I_{2z} - (1/2)(I_1^+ I_2^- + I_1^- I_2^+)] \quad (1)$$

where $\omega_i(t)$, $\omega_d(t)$ denote the periodic time-dependent coefficients (due to MAS) of the chemical shift and dipolar interactions, respectively. Such periodic time-dependent interactions may be conveniently expressed by a Fourier series expansion given below

$$\omega_\lambda(t) = \sum_{m=-2}^{2} \omega_\lambda^{(m)} e^{i2\pi m\nu_r t} \quad (2)$$

(51) Metz, G.; Wu, X.; Smith, S. O. *J. Magn. Reson. A* **1994**, *110*, 219−227.

where $\omega_\lambda^{(m)}$ (for $\lambda = 1$, 2, or d) denotes the time-independent Fourier component associated with a particular interaction. The orientation dependence[52] of the chemical shift interaction is expressed through the coefficients

$$\omega_\lambda^{(m)} = \omega_{\mathrm{iso}}^\lambda \delta_{m=0} + \omega_{\mathrm{aniso}}^\lambda \left\{ D^2_{0,-m}(\Omega_{PR}^\lambda) - \frac{\eta^\lambda}{\sqrt{6}}[D^2_{-2,-m}(\Omega_{PR}^\lambda) + D^2_{2,-m}(\Omega_{PR}^\lambda)] \right\} d^2_{-m,0}(\beta_{RL}) \quad (3)$$

where $\omega_{\mathrm{iso}}^\lambda = -\omega_0 \sigma_{\mathrm{iso}}^\lambda$ and $\omega_{\mathrm{aniso}}^\lambda = -\omega_0 \sigma_{\mathrm{aniso}}^\lambda$ represent the isotropic and anisotropic components of the interaction. The chemical shielding parameters (such as isotropic chemical shift, anisotropy, and asymmetry parameters) are related to the principal values of the shielding tensor according to $\sigma_{\mathrm{iso}}^\lambda = (1/3)(\sigma_{xx}^\lambda + \sigma_{yy}^\lambda + \sigma_{zz}^\lambda)$, $\sigma_{\mathrm{aniso}}^\lambda = \sigma_{zz}^\lambda - \sigma_{\mathrm{iso}}^\lambda$, and $\eta^\lambda = (\sigma_{yy}^\lambda - \sigma_{xx}^\lambda/\sigma_{zz}^\lambda - \sigma_{\mathrm{iso}}^\lambda)$, respectively. $D^2_{p,q}(\Omega_{PR}^\lambda)$ is an element of the Wigner rotation matrix (of rank 2) describing the transformation from the principal axis frame P^λ of the interaction λ through a given crystal fixed frame C (which in our case is chosen to coincide with the dipolar principal axis system) to the rotor frame R, i.e.,

$$D^2_{p,q}(\Omega_{PR}^\lambda) = \sum_{k=-2}^{2} D^2_{p,k}(\Omega_{PC}^\lambda) D^2_{k,q}(\Omega_{CR}^\lambda) \quad (4)$$

where $\Omega_{XY} = \{\alpha_{XY}, \beta_{XY}, \gamma_{XY}\}$ denotes the Euler angles relating the frames X and Y. Ω_{PC}^λ specifies the orientation of the interaction tensor relative to the crystal fixed frame and Ω_{CR}^λ represents the so-called powder angles describing the individual crystallite orientation relative to the rotor frame. The reduced Wigner matrix element $d^2_{-m,0}(\beta_{RL})$ relates the transformation from the rotor frame R to the laboratory frame L with $\beta_{RL} = \tan^{-1}(\sqrt{2})$ being the magic angle. The definition of the dipolar coefficients is analogous to the above description and is represented by

$$\omega_d^{(m)} = b_{jk} \sum_{m1=-2}^{2} D^2_{0,m1}(\Omega_{PC}^{jk}) \times D^2_{m1,m}(\Omega_{CR}^\lambda) d^2_{m,0}(\beta_{RL}) \quad (5)$$

where b_{jk} is the through-space dipole coupling constant given by $b_{jk} = (-(\mu_0/4\pi))\gamma^2\hbar(1/r_{jk}^3)$ in units of rad s^{-1}. For the sake of clarity and convenience, the above Hamiltonian is rewritten using the single transition operator basis.[53] In this basis the Hamiltonian is written as a sum of two interaction terms, namely,

$$H = H_0 + H_1 \quad (6)$$

where

$$H_0 = \omega_\Sigma(t) I_z^{14} + \omega_A(t)(I_z^{12} - I_z^{34}) \quad (7)$$

$$H_1 = \delta(t) I_z^{23} + \omega_B(t) I_x^{23} \quad (8)$$

and $\omega_\Sigma(t) = \omega_1(t) + \omega_2(t)$ and $\delta(t) = \omega_1(t) - \omega_2(t)$ denote the sum and the difference of the chemical shift terms. Since the exchange dynamics under the R^2 condition is described in the zero quantum subspace, the spin system is only governed by the interaction term H_1 and is represented by

$$H_1 = \delta I_z^{23} + \omega_B(t) I_x^{23} \quad (9)$$

where the time-dependent CSA coefficients have been omitted for the sake of simplicity and $\delta = \omega_1^{\mathrm{iso}} - \omega_2^{\mathrm{iso}}$ denotes the isotropic chemical shift difference between the spin pair of interest. To describe the observed interference effect between the MAS modulated spatial component (of the dipolar interaction) and the chemical shift modulated spin component of the interaction, the above Hamiltonian is transformed into an interaction frame (defined by the transformation function $U = \exp\{i(2\pi n v_r t) I_z^{23}\}$). In this frame, the Hamiltonian is represented by

$$H^T = U H_1 U^{-1} = (\delta - n v_r) I_z^{23} + \omega_B(t)[I_x^{23} \cos(2\pi n v_r t) + I_y^{23} \sin(2\pi n v_r t)] \quad (10)$$

Inserting the dipolar time-dependent coefficients in the above expression, the interaction Hamiltonian can be re-expressed as

$$H^T = (\delta - n v_r) I_z^{23} + \sum_{m=-2}^{2} \omega_B^{(m)}[I_+^{23} e^{i(n-m)2\pi v_r t} + I_-^{23} e^{i(n+m)2\pi v_r t}] \quad (11)$$

which can further be simplified to

$$H^T = (\delta - n v_r) I_z^{23} + |\omega_B^{(n)}| I_x^{23} \quad (12)$$

So far, we have neglected the time-dependence of the chemical shift anisotropy. Although it is true that the CSA interaction would affect the line shape of cross-peaks of a correlation spectrum, their effect on polarization transfer is less significant.[54] The unitary operator described above may be modified to include the time-dependent CSA interaction and has been described in detail by Karlsson et al.:[48]

$$U(t) = \exp\{-i[2\pi n v_r t + \Phi_\Delta^{\mathrm{aniso}}(t,0)] I_z^{23}\} \quad (13)$$

where

$$\Phi_\Delta^{\mathrm{aniso}}(t_a,t_b) = \int_{t_a}^{t_b} \omega_\Delta^{\mathrm{aniso}}(t)\, \mathrm{d}t$$

In this frame the Hamiltonian is represented by

$$H^T = (\delta - n v_r) I_z^{23} + \tilde{\omega}_B(t) I_x^{23} \quad (14)$$

where $\tilde{\omega}_B(t) = \omega_B(t) \exp[-i\Phi_\Delta^{\mathrm{aniso}}(t,0)]$. Usually, the exchange dynamics is governed by the interaction Hamiltonian and depends on the experimental scheme employed. In the conventional R^2 experiments ($\delta = n v_r$) the above interaction Hamiltonian has only a transverse component and is purely dipolar in nature, whereas in the case of R^{2}W experiments, since the exchange dynamics is monitored as a function of spinning frequency, the interaction Hamiltonian has both the longitudinal (described by the resonance mismatch terms) as well as a transverse component (described by the dipolar terms). Since the exchange dynamics are influenced by both coherent (described by the Hamiltonian operator) as well as incoherent interactions (described by the relaxation operator), the spin dynamics is best studied by using the Liouville formalism. In this approach, a new set of basis operators are defined (also known as super-operators) and the time evolution of the spin system (represented by the spin density operator, $\rho(t)$) is studied by solving the Liouville-von Neumann equation

$$\frac{\mathrm{d}}{\mathrm{d}t}\rho(t) = -i[H,\rho(t)] - \hat{\Gamma}\rho(t) \quad (15)$$

Using the Liouville super-operator $\hat{L}$ (represented by $\hat{L} = -i\hat{H} - \hat{\Gamma}$), the above equation can be further simplified and rewritten as a first-order homogeneous differential equation

$$\frac{\mathrm{d}}{\mathrm{d}t}\rho(t) = \hat{L}\rho(t) \quad (16)$$

The term $\hat{H}$ in the Liouville super-operator $\hat{L}$ denotes the Hamiltonian

(52) Spiess, H. W. In *Dynamic NMR Spectroscopy*; Diehl, P., Fluck, E., Kosfeld, R., Eds.; Springer-Verlag: Berlin, 1978; Vol. 15, pp 55−214.
(53) Vega, S. *J. Chem. Phys.* **1978**, *68*, 5518.
(54) Duma, L., Hediger, S., Lesage, A., Sakellariou, D.; Emsley, L. *J. Magn. Reson.* **2003**, *162*, 90−101.

commutation super-operator whose matrix elements are defined by

$$\hat{H}_{ab} = \langle Q_a|\hat{H}|Q_b\rangle = Tr\{Q_a{}^{+}[H,Q_b]\} \tag{17}$$

where $|Q_a\rangle$,$|Q_b\rangle$ etc. are orthonormal basis operators defined in the Liouville space and $\hat{\Gamma}$ denotes the relaxation super-operator, which is usually diagonal for all practical purposes (neglecting cross-relaxation terms) and is formally represented by

$$\hat{\Gamma} = \sum_i \frac{|Q_i\rangle\langle Q_i|}{T^{(i)}\langle Q_i|Q_i\rangle} \tag{18}$$

The term T^i in the above equation denotes the relaxation time associated with a given coherence *i*. In the R^{2}W experiments described here, the relevant Liouville subspace is spanned by the operators $\{|I_{1z}\rangle,|I_{2z}\rangle,|\sqrt{2}I_x^{23}\rangle,|\sqrt{2}I_y^{23}\rangle\}$ and the Liouville super-operator $\hat{L}$, is represented by a 4 × 4 matrix. This representation of the Liouville super-operator is due to the fact that the R^{2}W experiments described here involve a polarization transfer from spin 1 to spin 2 (which is not polarized initially). Moreover, the relaxation rates associated with a particular coherence can be directly related to the longitudinal relaxation times. Using the explicit form of the operators mentioned above, eq 14 can be expanded as follows

$$\frac{d}{dt}\begin{pmatrix}\langle I_{1z}(t)\rangle\\ \langle I_{2z}(t)\rangle\\ \langle\sqrt{2}I_x^{23}(t)\rangle\\ \langle\sqrt{2}\,I_y^{23}(t)\rangle\end{pmatrix} = \begin{pmatrix}\left(-\frac{1}{T_1^{(1)}}\right) & 0 & 0 & \sqrt{2}\omega_B^n\\ 0 & \left(-\frac{1}{T_1^{(2)}}\right) & 0 & -\sqrt{2}\omega_B^n\\ 0 & 0 & \left(-\frac{1}{T_2^{ZQ}}\right) & -(\delta - n\upsilon_r)\\ -\sqrt{2}\omega_B^n & \sqrt{2}\omega_B^n & (\delta - n\upsilon_r) & \left(-\frac{1}{T_2^{ZQ}}\right)\end{pmatrix} \begin{pmatrix}\langle I_{1z}(t)\rangle\\ \langle I_{2z}(t)\rangle\\ \langle\sqrt{2}I_x^{23}(t)\rangle\\ \langle\sqrt{2}I_y^{23}(t)\rangle\end{pmatrix} \tag{19}$$

Here, $T_1^{(i)}$ denotes the longitudinal relaxation time associated with spin *i* and is determined experimentally by measuring the intensity (or magnetization) as a function of mixing time far from rotational resonance conditions. In our case, the measured $T_1^{(i)}$ were long and have been neglected in the calculations. The term T_2^{ZQ} refers to the zero quantum relaxation parameter and accounts for effects that are not directly correlated to the chemical shift or the dipolar interactions. The spin dynamics are then evaluated by solving eq 19. Usually, the distance information for a particular spin pair is obtained by calculating the root-mean-square deviation between the experimental and simulated data that is represented as

$$\text{RMSD} = \frac{1}{N}\sum_{i=1}^{N}(E^i - S^i)^2 \tag{20}$$

Here E^i and S^i denote the experimental and simulated data (integrated cross-peak intensities in our case) for a particular spin pair of interest. The summation index here refers to the number of experiments (denoted by *N*, corresponding to different sample spinning frequencies) performed. The internuclear distance *r* and the zero-quantum relaxation T_2^{ZQ} constitute the fit parameters in such calculations.

Data Analysis. The experimental data from the R^{2}W experiments were processed using NMRPipe,[55] and the cross-peak volumes were extracted by automated fitting to two-dimensional Gaussians. Analysis of the magnetization exchange curves involved: (i) normalization of all data points to initial carbonyl intensities derived from cross-polarization reference experiments conducted at identical spinning frequencies to compensate for the dependence of CP enhancements on the sample spinning frequency, (ii) normalization of cross-peak volumes to carbonyl intensity at a spinning frequency which is free from any recoupling conditions, and (iii) estimation of model parameters using a Liouville-space formalism (Equation 19) of the spin dynamics (vide supra) which considers only two coupled spins. For model estimation, the root-mean-square deviation between the calculated and measured

(55) Delaglio, F.; Grzesiek, S.; Vuister, G. W.; Pfeifer, J.; Bax, A. *J. Biomol. NMR* **1995**, *6*, 277−293.

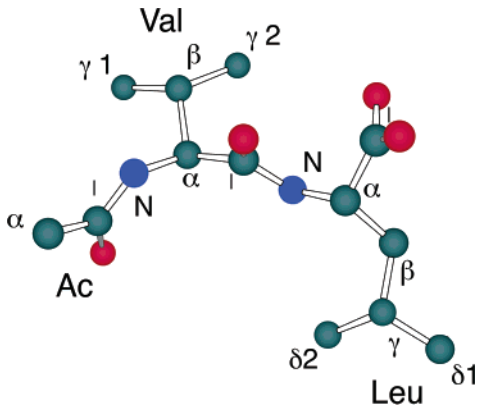

Figure 2. Diagram of the peptide *N*-Ac-Val-Leu derived from the crystal structure. The nomenclature used to label measured distances in the text is indicated.

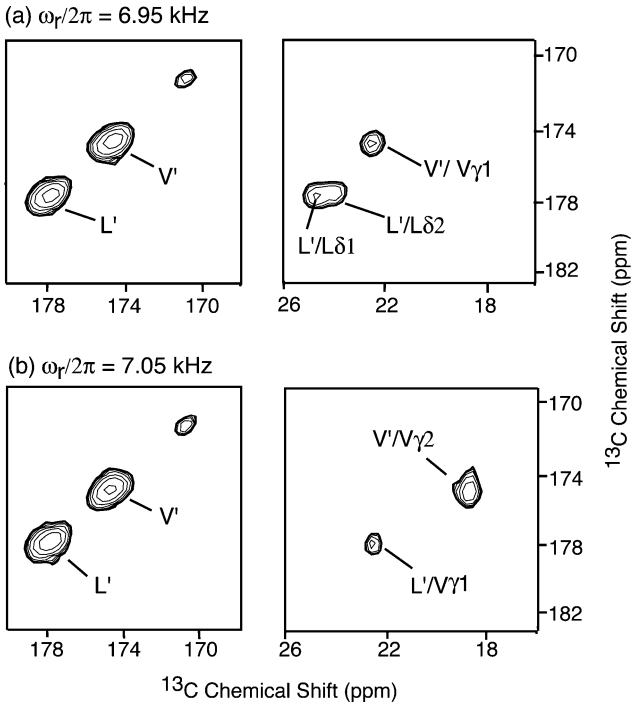

Figure 3. Representative two-dimensional slices from the $^{13}C-^{13}C$ R^{2}W experiment in *N*-acetyl [U-^{13}C,^{15}N]-L-Val-L-Leu recorded on a 360-MHz spectrometer at (a) $\omega_r/2\pi = 6.95$ kHz and (b) $\omega_r/2\pi = 7.05$ kHz. The pulse sequence of Figure 1b was used with the mixing time of 30 ms. Different cross-peaks appear at different spinning frequencies, thereby demonstrating the selectivity of the polarization transfer. In (a) cross-peaks corresponding to the medium range V′−Vγ1 dipolar coupling ($R = 3.879$ Å according to the crystal structure) appear in the spectrum, along with long-range couplings between the L′−Lδ1 ($R = 4.675$ Å) and L′−Lδ2 ($R = 4.872$ Å). These cross-peaks are not present in (b) (note that the spinning frequency changes by just 100 Hz), but two additional cross-peaks appear between L′ and Vγ1 ($R = 6.464$ Å) and V′ and Vγ2 ($R = 2.969$ Å).

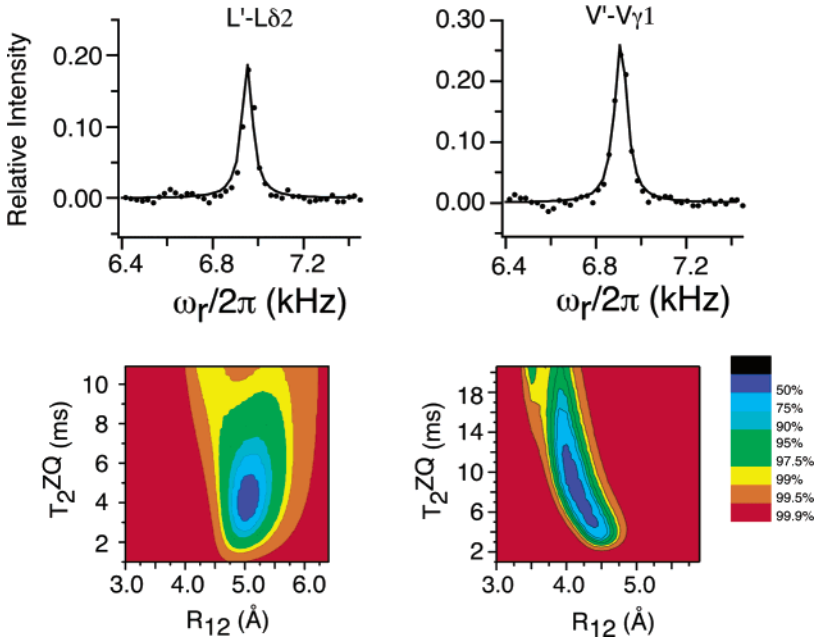

Figure 4. Representative plots of the cross-peak intensities as a function of the spinning frequency for the L′−Lδ2 and V′−Vγ1 rotational resonances and corresponding graphs of the model estimator in which contour levels are confidence intervals determined from an F-test. The volume intensities of the cross-peaks are given relative to the corresponding carbonyl peaks. The parameters in the best fit simulations were as follows. For L′−Lδ2: $T_2^{ZQ} = 4.0$ ms, $R = 5.0$ Å. For V′-Vγ1: $T_2^{ZQ} = 8.9$ ms, $R = 4.25$ Å. The confidence limits of the contour levels are indicated on the figure.

magnetization exchange curves was minimized; confidence intervals reflected in the contour plots were derived on the basis of an F-test[56] in which only points above the noise floor were used to enumerate the degrees of freedom in the model fitting. The experimental details and results obtained using this method are discussed in the next section.

Results and Discussion

To validate our approach, the proposed 3D R^2W experiment was applied to carbonyl side chain distance measurements in *N*-acetyl-[U-^{13}C,^{15}N]L-Val-L-Leu. The three-dimensional structure of this dipeptide had been previously determined using X-ray crystallography[57] and is illustrated in Figure 2. In combination with 2D ^{13}C−^{13}C correlation spectroscopy, the R^2W methodology allows the measurement of multiple distance constraints in a site-specific manner.

The R^2W experiments were performed at 360 MHz (^{1}H frequency) and at spinning frequencies ranging from 5.8 to 7.5 kHz, incremented in steps of 25 Hz. The sweep range of the sample spinning frequencies employed in the 2-D experiments were chosen to satisfy appropriate resonance conditions ($n = 2$) between all carbonyl and side-chain carbons. Figure 3 illustrates representative two-dimensional slices from the R^2W experiment corresponding to spinning frequencies of 6.95 and 7.05 kHz and to a mixing time of 30 ms.

The cross-peaks in the aliphatic region are labeled with the carbonyl and side-chain carbon frequencies. When the spinning frequency corresponds or is sufficiently close to the R^2 condition for a particular carbonyl−side chain spin pair, the magnetization exchange between the spins results in the appearance of cross-peaks in the aliphatic region of the spectrum. The aliphatic regions of the spectra demonstrate that these polarization exchange processes are highly selective. In particular, at $\omega_r/2\pi = 6.95$ kHz, the V′−Vγ1 (medium-range; $R = 3.879$ Å according to crystal structure), L′−Lδ1 (long-range; $R = 4.675$ Å), and L′−Lδ2 (long range; $R = 4.872$ Å) interactions are recoupled. However, at a slightly higher spinning frequency, $\omega_r/2\pi = 7.05$ kHz, the corresponding cross-peaks disappear, and cross-peaks corresponding to L′−Vγ1 (long range; $R = 6.46$ Å), and V′−Vγ2 (short-range; $R = 2.969$ Å) appear. The varying cross-peak intensities associated with a particular spin pair of interest provide a measure of polarization transfer as a function of sample spinning frequency and can be used as a tool to estimate the distance between the spins of interest. The dependence of the cross-peak intensity on the spinning frequency is shown in Figure 4 for the L′−Lδ2 and V′−Vγ1 spin pairs together with the best-fit simulations and confidence plots. The T_1 relaxation times were calibrated in separate experiments. In all the experiments described in this article, the peak intensities were referenced with respect to the intensity of the carbonyls (that were polarized initially). In addition, the above intensities were corrected for the dependence of CP enhancement on the sample spinning frequency. The experimentally observed polarization transfer efficiency is quite high for stronger coupling and is on the order of 20% for longer (L′−Lδ2) distances. Using the numerical procedure described in the previous section and from the RMSD plots, a total of nine distances were extracted with high precision and are presented in Table 1 and Figure 5. As is clear from the table, the distances measured using NMR are in good agreement with X-ray data, despite the fact that multispin effects have been neglected in our calculations. The agreement between the two data sets further justifies our use of a simplified two-spin model for data analysis. It also is in agreement with the earlier reported effect of the reduction of dipolar truncation in the presence of multiple quantum relaxation.[58] Although multiple spins on the exchange dynamics seem

(56) Shoemaker, D. P.; Garland, C. W.; Nibler, J. W. *Experiments in Physical Chemistry*; McGraw-Hill: New York, 1989.
(57) Carroll, P. J.; Stewart, P. L.; Opella, S. J. *Acta Crystallogr.* **1990**, *C46*, 243−246.
(58) Ladizhansky, V.; Griffin, R. G. *J. Am. Chem. Soc.* **2003**, *in press*.

Table 1. $^{13}C-^{13}C$ Internuclear Distances and ZQ Relaxation Times Determined in *N*-Ac-L-Val-L-Leu

atoms		$^{13}C-^{13}C$ distance, Å		
		R^2W^a	X-ray	T_2^{ZQ}, ms
V	Vγ2	3.20 ± 0.20	2.969	5.9
	Vγ1	4.25 ± 0.35	3.879	8.9
	Lδ1	4.40 ± 0.70	4.290	13.0
	Lβ	3.25 ± 0.45	3.715	9.3
L	Vγ2	4.80 ± 0.70	4.535	4.3
	Vγ1	6.50 ± 0.80	6.460	0.1[b]
	Lδ1	5.00 ± 0.60	4.675	6.0
	Lδ2	5.10 ± 0.50	4.872	4.0
	Lβ	2.95 ± 0.45	2.487	7.0

[a] The error bars are given with 95% confidence level. [b] The R^2W data for L′−Vγ1 spin pair could be fitted with T_2^{ZQ} relaxation 0.1−10 ms. The polarization transfer efficiency for this cross-peak was very weak because of the long distance and could be fitted with broad distribution of the ZQ relaxation parameter.

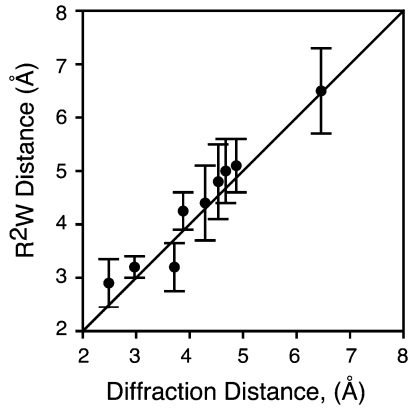

Figure 5. Comparison of $^{13}C-^{13}C$ distances measured by using X-ray diffraction and R^2W experiments. NMR results account for random errors.

to be less significant in our case, their effects may become prominent when studying larger biomolecules such as proteins and peptide aggregates. However, such multispin effects can be minimized due to better chemical shift resolution at higher field strengths.

To investigate other sources of systematic error, the dependence of the spin dynamics on the magnitude and orientation of the CSA was studied. For a given set of model CSA parameters,[59] a series of numerically exact simulations were performed and then fitted using the approximate treatment presented here. The results of the simulations indicate an overestimation of the internuclear distances of at worst 0.2 Å using NMR when the CSA parameters are not known *a priori*. Such dependence on CSA parameters can, however, be minimized at the $n = 1$ R^2 condition.

One of the limitations of this approach is the stringent condition imposed on the sample spinning frequency. This restricts the applicability of this technique to systems in which the CSA's are small compared to the chemical shift differences. Where this condition is not met, the resolution is often obscured by the presence of crowded sidebands, which in turn affects the selectivity. Such problems can be partially alleviated by employing the R^2TR technique (rotational resonance in the tilted frame) introduced by Terao et al.[40,41] This approach relaxes the restrictions on the sample spinning frequency in addition to eliminating the broadening effects observed under rotational resonance conditions.

Conclusions

We have demonstrated the application of the 3-D R^2W technique for simultaneous site-specific measurement of multiple $^{13}C-^{13}C$ (carbonyl−side chain) distances in uniformly ^{13}C-labeled solids. The method relies on ^{13}C chemical shift resolution and is expected to benefit from higher static magnetic fields with better selectivity and reduced dependence on multispin effects. Since the recoupling is chemical shift-modulated, its application is limited to systems with spin pairs having significant isotropic chemical shift differences. Fortunately, many interesting biological systems satisfy this criterion. Further, the effects of dipolar truncation are significantly reduced in this approach and enable the extraction of distance constraints even in weaker (or long range) couplings. Moreover, in systems with favorable chemical shift resolution, the distance information can be extracted without ambiguity using a simple two-spin approximation model. Thus, the reduced dependence on relaxation and other multispin parameters makes this a suitable approach for measuring distances in larger uniformly labeled biological systems.

Acknowledgment. This work was supported by grants from the National Institute of Health (GM-23403 and R.R.-00995). V.S.B. acknowledges the receipt of a postgraduate fellowship from the Natural Sciences and Engineering Research Council of Canada.

Note Added after ASAP: The version published on the Web 11/21/2003 contained errors in eqs 12 and 18 and in citation of ref 38. The final Web version published 11/24/2003 and the print version are correct.

JA037761X

(59) Ye, C.; Fu, R.; Hu, J.; Ding, S. *Magn. Reson. Chem.* **1993**, *31*, 699.